Macromolecules

pubs.acs.org/Macromolecules Article

Ionic Effect on Electrochemical Behavior of Water-Soluble Radical Polyelectrolytes

Yanlin Shi,[‡] Chanaka J. Mudugamuwa,[‡] Thidas N. Abeysinghe, Yasser S. M. Alotaibi, Michael J. Monteiro, Justin M. Chalker, Jodie L. Lutkenhaus, and Zhongfan Jia*

Cite This: *Macromolecules* 2022, 55, 5733–5743 Read Online

ACCESS | Metrics & More | Article Recommendations | Supporting Information

ABSTRACT: Water-soluble redox-active polymers (RAPs) have emerged as attractive electroactive materials for aqueous redox flow batteries because these systems rely on readily available size-exclusion membranes rather than expensive ion-selective membranes. While incorporating ionic units is the most effective strategy for forming water-soluble redox polyelectrolytes, little is known about how charges dictate their electrochemical behavior. Here, we design a series of water-soluble TEMPO (2,2,6,6-tetramethylpiperidyl-1-oxy) radical polyelectrolytes with identical radical distribution but various ionic groups through a sequential postmodification method. Physical and electrochemical characterizations show disparate diffusion coefficients (D) and charge transfer kinetics (k^0) of these radical polyelectrolytes at various pH. Particularly, pH exerts a strong impact on k^0 of the negatively charged polymer (i.e., with carboxylic acid groups). The bimolecular reaction rate k_{ex} determined from redox-induced polymer films shows electrostatic interactions between charged segments can enhance the electron self-exchange reaction rate by ten folds. The results suggest that charge effects are of great importance when designing water-soluble redox polymers for electrochemical applications.

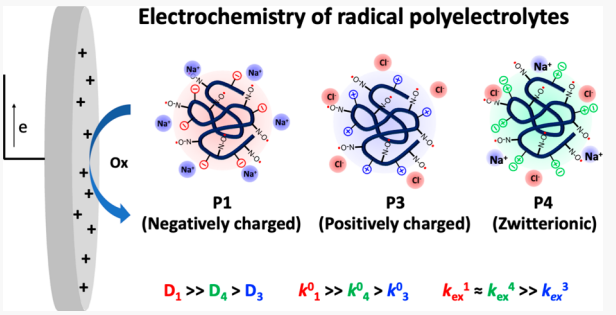

INTRODUCTION

Aqueous redox flow batteries (ARFBs) have emerged as large-scale and safe energy storage systems that are ideal for storing renewable energy from solar or wind farms.[1−5] However, when traditional inorganic and small organic redox-active compounds are employed as electroactive materials, ARFBs require the use of expensive ion-selective membranes (i.e., Nafion), which account for up to 40% of the total cost.[6,7] In contrast, redox-active polymers (RAPs) possess high molecular weights and large hydrodynamic volumes,[8] which enable polymer-based ARFBs to use more cost-effective semipermeable membranes, such as dialysis membrane. The controlled pore size of the membrane prevents polymers from crossing over while allowing rapid ion diffusion.[9−11] Since many organic redox-active molecules are hydrophobic, the corresponding polymers are often water-insoluble or have very low water solubility. Therefore, incorporating hydrophilic units to make redox-active copolymers water-soluble is essential for polymer-based ARFBs.[11]

Polyelectrolytes are generally water-soluble, forming charged polymer chains surrounded by dissociated counterions.[12,13] In many cases, their chain conformations and charge states vary with pH,[14] ionic strength,[15] and electrostatic interactions.[16] One interesting behavior of polyelectrolytes is their movement driven by an external electric field, which is the basis of the well-known gel electrophoresis techniques for analyzing charged biopolymers, such as DNA and proteins. In the past two decades, polyelectrolytes have emerged as functional materials for antifouling coatings,[17] ultrafast responsive electronics,[18] and solid polyelectrolyte membranes in high-capacity batteries and fuel cells.[19] Inspired by polyelectrolytes, ionic monomers can be incorporated into RAPs to form a class of water-soluble, redox-active polyelectrolytes. The first example of using this type of polymers in an ARFB was demonstrated by Schubert and co-workers who exemplified the synthesis of positively charged RAPs as catholyte and anolyte.[11] Recent work from the same group reported another water-soluble RAP by incorporating a zwitterionic comonomer.[20] The water solubility of RAPs could also be improved through the addition of water-soluble neutral monomers, such as oligopoly(ethylene glycol) acrylate.[21] Evaluation of ARFBs consisting of these materials has shown great promise with the benefit of using low-cost, semipermeative membranes.

It is known that electric fields can dictate the migration, deposition, desorption, and multilayer formation on electrode

Received: March 13, 2022
Revised: June 4, 2022
Published: July 1, 2022

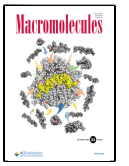

https://doi.org/10.1021/acs.macromol.2c00519
Macromolecules 2022, 55, 5733−5743

Scheme 1. Synthesis of Radical Polyelectrolytes with Different Charges through a Sequential Post-polymerization Modification

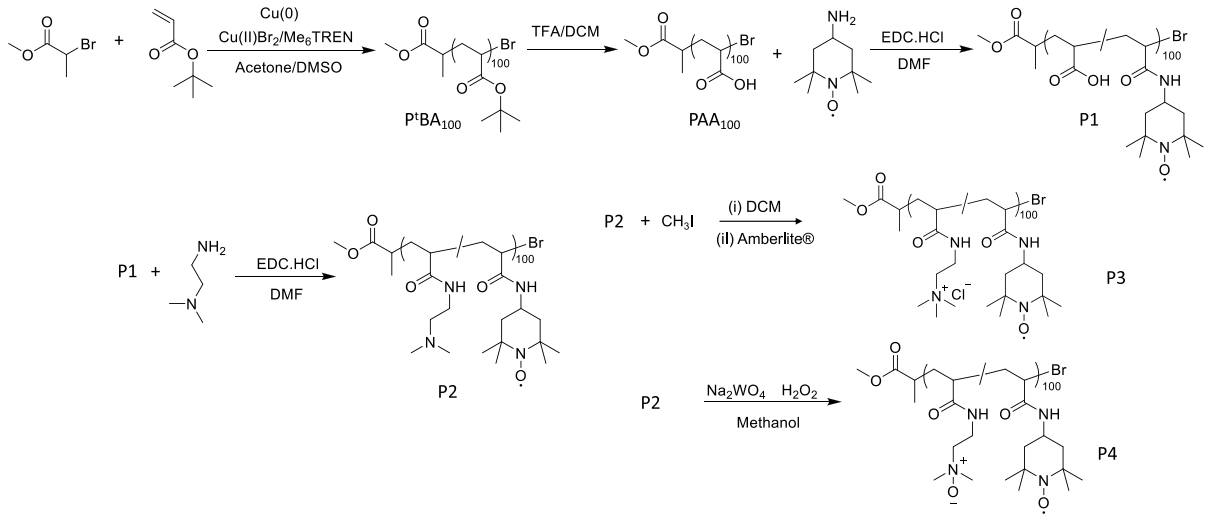

surfaces.[22,23] Early theoretical studies by Netz[16] using dynamic simulations determined a critical electric field required for unfolding a collapsed polyelectrolyte chain. The work also revealed that the electric field controlled the movement of polyelectrolyte chains and associated counterions. When incorporating redox-active groups, the resulting polyelectrolytes under certain potential bias will show a Faradaic electrochemical activity and could still experience an electrostatic force (even the electric field strength would be weaker than the electrophoresis). Although there is great interest in the electrochemical reactivity of redox-active polyelectrolytes, studies on their electrochemical kinetics, however, are mostly carried out in organic solvents for nonaqueous RFBs.[10,24] For example, Rodriguez-Lopez and co-workers studied the electrochemical kinetics of RAPs in organic electrolytes with a particular interest in the effect of ionic strength and salt concentration.[25] Using positively charged viologen-based RAPs as examples, the authors found that the increased salt concentration in an acetonitrile electrolyte can drive chain collapse and RAP adsorption on the electrode surface. The change of hydrodynamic radii of polyelectrolytes resulted in the change of solution viscosity hence the diffusion and charge transfer even at 10:1 ratio of supporting electrolytes to active species. These seminar work suggest a very different behavior of redox-active polyelectrolytes to those small molecular counterparts. Nevertheless, little is known about how different charges on redox-active polyelectrolytes dictate their redox performance in an aqueous media at various pH, which is of great significance to their application in ARFBs.

To this end, we have designed a library of redox-active polyelectrolytes containing pendant 2,2,6,6-tetramethylpiperidyl-1-oxy (TEMPO) groups—stable radical species with well-defined redox activity and widespread use in polymer-based energy storage.[26] The postpolymerization modification method was used to convert poly(*t*-butyl acrylate) (P^tBA) to a panel of radical polyelectrolytes containing negatively charged, positively charged, or zwitterionic groups (Scheme 1). The sequential modification method affords these polymers with the same proportion and distribution of TEMPO groups, but different ions. This strategy was designed to understand the constitutional impact of charges on electrochemical behavior of these radical polyelectrolytes. We applied dynamic light scattering (DLS), cyclic voltammetry (CV), and linear sweep voltammetry (LSV) with rotating disk electrode (RDE) techniques to extrapolate the diffusion, adsorption, and electron transfer kinetics of these polymers. We discovered that the ionic states strongly influence the electrochemical redox behaviors of these radical polyelectrolytes, suggesting the critical importance of ions in designing and applying RAPs for ARFBs.

EXPERIMENTAL SECTION

Materials. The inhibitor in *tert*-butyl acrylate (tBA, Aldrich, >99%) was removed before use by passing through a basic alumina column. The following reagents were used as received: alumina, activated basic (Aldrich, rockmann I, standard grade, ~150 mesh, 58 Å), triethylamine (TEA, Fluka, 98%), trifluoroacetic acid (TFA, Aldrich, ≥99.0%) silica gel 60 (230−400 mesh) ATM (SDS), TLC plates (silica gel 60 F254), sodium chloride (Univar, 99.9%), hydrogen peroxide 30% w/w (Univar, AR grade), *N*-(3-(dimethylamino)propyl)-*N*′-ethylcarbodiimide hydrochloride (EDC·HCl, Aldrich, 97%), 4-amino-2,2,6,6-tetramethylpiperidine (Aldrich, 98%), *N*,*N*-dimethylethylenediamine (Aldrich 95%), iodomethane (Aldrich, 99%), and acetic anhydride (Chem Supply). All the common solvents were AR grade and used as received. The following initiators, ligands, and metals for polymerizations were used as received unless otherwise stated. Methyl-2-bromopropionate (MBP, Aldrich, 98%), copper(II) bromide ($CuBr_2$, Aldrich, 99%), fresh polished copper wire (d = 0.5 mm). Buffer solutions used in this work were 0.1 M PBS (pH 5.8 and 7.3) and carbonate buffer (pH 9.0). pH values of all buffer solutions were measured by a Hanna pH meter.

Synthesis of Radical Polyelectrolytes. *Synthesis of Negatively Charge Radical Polyelectrolyte P1.* PAA (2.0 g, 27.75 mmol carboxylic acid) was weighed to a 250 mL flask and dissolved with DMF (50 mL). EDC·HCl (3.99 g, 20.71 mmol) was added to the above solution, which was cooled with an ice-bath. 4-Amino-TEMPO (2.85 g, 16.65 mmol, 0.6 equiv to carboxylic acid) was dissolved in DMF (50 mL) and, then, was added to the above PAA/DMF solution dropwise by a constant pressure funnel within 30 min. Two days later, the reaction solution was concentrated by airflow to remove most of DMF and then dialyzed against ethanol to remove remaining DMF. After dialysis, the solution was concentrated, precipitated in diethyl ether, and filtered to obtain the product as a pink powder, which was dried under a high vacuum at 25 °C (3.8 g, yield = 84%).

Synthesis of Tertiary Amine Functional Radical Polymer P2. The polymer P1 (1.98 g) was added to a 50 mL flask and dissolved in 20 mL of DMF. EDC·HCl (3.51 g, 18.32 mmol) was added to the above solution and cooled with an ice-bath. *N*,*N*′-dimethylethylenediamine

https://doi.org/10.1021/acs.macromol.2c00519
Macromolecules 2022, 55, 5733−5743

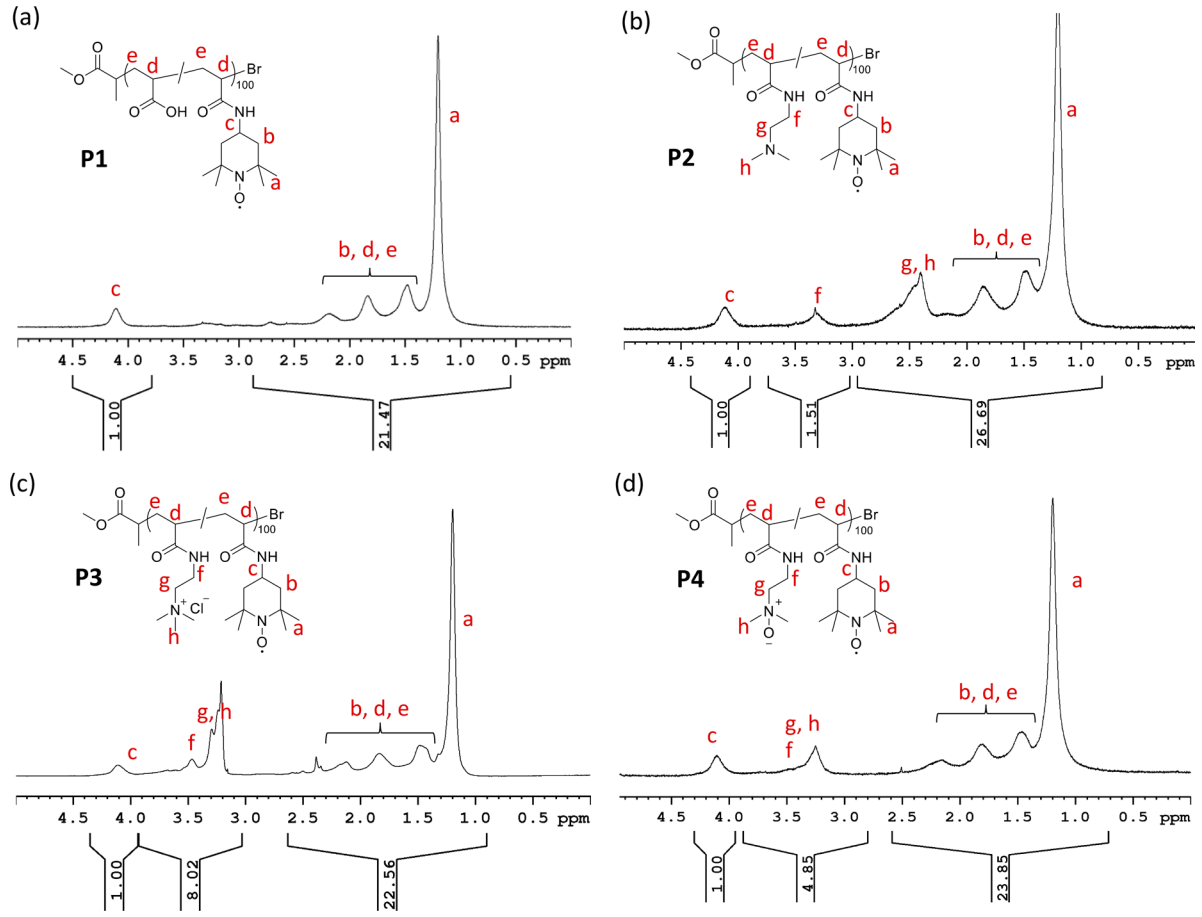

Figure 1. ^{1}H NMR spectra of radical polyelectrolytes (a–d, P1–P4) in methanol-d_4 in the presence of a catalytic amount of Pd/C and ammonium formate.

(1.29 g, 14.63 mmol) was dissolved in 10 mL DMF and, then, was added to the above solution using a dropping funnel. Forty-eight hours later, the reaction solution was dialyzed against MeOH/H_2O (v/v = 20/80) and then dialyzed against EtOH. Finally, the solution was concentrated and precipitated in diethyl ether to obtain the product as a pink powder, which was dried under a high vacuum at 25 °C (2.23 g, yield = 74%).

Synthesis of Positively Charged Radical Polyelectrolyte P3. The polymer P2 (0.3 g) was dissolved with 3 mL of DCM in a 20 mL vial. Iodomethane (0.13 g) in 1 mL of DCM solution was added to the above polymer solution dropwise. Four hours later, the polymer precipitated out, and the solvent was removed under airflow. The polymer was dissolved in 3 mL of H_2O, and the Amberlite IRA-900 chloride form was added to replace the iodide ion with the chloride ion. The solution was filtered through the cotton and then freeze-dried to obtain the product (0.265 g).

Synthesis of Zwitterionic Radical Polyelectrolyte P4. The polymer P2 (0.4 g) was dissolved in 5 mL of MeOH, and Na_2WO_4 (0.05 g, 0.17 mmol) was added. Then, hydrogen peroxide (30% solution, 0.3 mL) was slowly added, and the reaction was allowed to proceed for 24 h. The reaction solution was dialyzed against DI water and freeze-dried to obtain red powder (0.32 g).

Structure Characterizations. *Size Exclusion Chromatography (SEC).* P^{t}BA was dissolved in THF and filtered by using a 0.45 μm PTFE syringe filter. Analysis of the molecular weight distributions of the polymers was accomplished using a Waters 2695 separations module, fitted with a Waters 410 refractive index detector at 25 °C. All samples were eluted in THF at a flow rate of 0.2 mL min^{-1}. Calibration was performed using narrow distribution polystyrene standards ($Đ$ < 1.1) ranging from 500 to 2 million g mol^{-1}.

Fourier Transform Infrared (FT-IR) Spectroscopy. FT-IR spectra were recorded on Thermo Nicolet Nexus 870 ESP FT-IR/NIR Spectrometer. Spectra were recorded between 4000 and 500 cm^{-1} by acquiring 64 scans at 4 cm^{-1} resolution. Without further sample preparation, solid power samples were pressed directly onto the diamond internal reflection element for measurements.

Nuclear Magnetic Resonance (NMR) Spectroscopy. All ^{1}H NMR spectra were recorded on a Bruker 500 MHz at 25 °C using an external lock (methanol-d_4) and referenced to the residual non-deuterated solvent.

Dynamic Light Scattering (DLS). Characterizations of polymer solutions were carried out on a Malvern ZetaSizer NS. Radical polyelectrolytes were dissolved in 0.1 M buffer at 10 mg/mL and filtered through 0.2 μm syringe filter to remove dust. The solution was transferred to a DTS1070 cell for size and zeta potential measurements. The detection angle was 173° backscatter. Data were averaged based on three measurements.

Electrochemical Methods. Electrochemical characterization, including cyclic voltammetry (CV), linear scan voltammetry (LSV) at a rotating disk electrode (RDE), and chronoamperometry (CA), were carried out on a Gamry Interface 1010E potentiostat (Warminster, PA, USA) using a standard three-electrode cell equipped with an ALS RRDE-3 rotating disk working electrode (BAS Inc. Tokyo, Japan). A platinum wire was used as a counter electrode and a Ag/AgCl as a reference electrode. The glassy carbon working electrode with a diameter of 3 mm was polished with Al_2O_3 power (0.05 μm) and rinsed with Mini-Q water and acetone before use. Radical polyelectrolytes (15–18 mg) were dissolved in 1 mL of water, out of which 200 μL was taken and diluted in 10 mL of 0.1 M PBS buffer solution at pH of 5.8, 7.3 and carbonate buffer pH of 9.0, resulting in a TEMPO radical concentration of 1 mM. The ionic

https://doi.org/10.1021/acs.macromol.2c00519
Macromolecules 2022, 55, 5733–5743

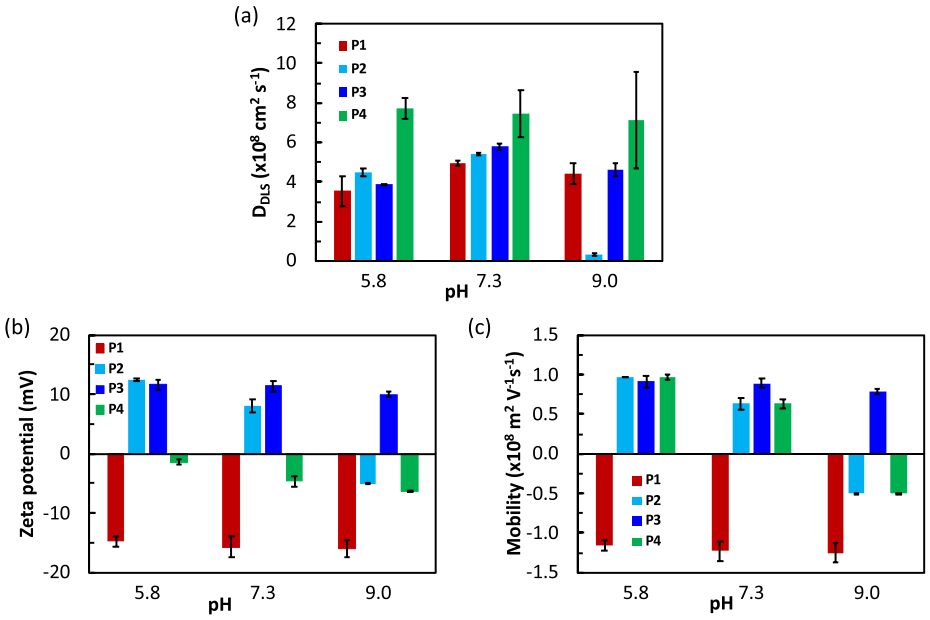

Figure 2. Solution characterization of radical polyelectrolytes in different buffer solutions using ZetaSizer, (a) Diffusion coefficient (D_{DLS}), (b) zeta potentials, and (c) electrophoresis mobility of P1−P4 at the concentration of 1 mg mL^{-1}. Buffer solution: 0.1 M PBS buffer at pH 5.8, 7.3, and 0.1 M carbonate buffer pH 9.0.

strength of these buffers was 0.22, 0.33, and 0.22 mol/L for pH of 5.8, 7.3, and 9.0, respectively. For RDE measurement, the rotating speed varied from 400 to 2000 rpm.

For adsorption experiments, a freshly polished GC working electrode was used to run a CV experiment of radical polyelectrolyte solution (1 mg/mL in 0.1 M pH 9.0 buffer) at a scan rate of 50 mV s^{-1} for 10 cycles. The electrode was then carefully rinsed with Milli-Q water and immersed in a blank pH 9.0 buffer to run the CV and CA experiments. When switching between different polymers, the working electrode was polished with Al_2O_3 power (0.05 μm), rinsed with Mini-Q water, and a CV was run to ensure no bound polymers were leftover before the next measurement.

The absorbed thin layer undergoes a reversible redox reaction. The observed peak current is symmetrical with a very small peak-to-peak gap. The electroactive coverage, Γ (mol cm^{-2}), can be calculated according to the equation $I_p = \frac{n^2F^2A\Gamma\upsilon}{4RT}$, where n is the number of electrons, F is the Faradaic constant, A is the electrode surface area (cm^2), ν is potential scan rate (V s^{-1}), R is the gas constant, and T is the temperature (298 K). From the slopes in d−e, surface concentration Γ (mol cm^{-2}) can be calculated. Charge density (μC cm^{-2}) = 10^3*F*Γ.

RESULTS AND DISCUSSION

Synthesis and Structural Characterizations of Radical Polyelectrolytes. Radical polyelectrolytes with pendant TEMPO groups were synthesized through a sequential, postpolymerization modification method. First, P^{t}BA$_{100}$ with 100 repeating units was obtained by Cu(0)-mediated single-electron transfer radical polymerization (SET-LRP),[27] a living polymerization technique that can control the chain length with narrow dispersity ($Đ$). Size exclusion chromatography (SEC) showed a number-average molecular weight of 16 160 g/mol and $Đ$ of 1.06 (Figure S1). P^{t}BA$_{100}$ was readily converted to poly(acrylic acid) (PAA$_{100}$) in the presence of trifluoroacetic acid (Figure S2). PAA was then used as a parent polymer to couple with 4-amino-TEMPO (see Supporting Information) and convert 60% of the carboxylic acid groups to TEMPO functional amide. The unmodified carboxylate groups impart negative charges to the radical polyelectrolyte (P1) (Scheme 1). ^{1}H NMR spectra (Figure 1) of all radical polymers were recorded in deuterated methanol in the presence of Pt/C and ammonium formate to reduce the radical to its hydroxylamine form. From the ^{1}H NMR spectrum of P1, the new peak at 4.15 ppm compared to PAA indicated the successful conjugation of TEMPO radicals (Figures 1a and S2). The calculated grafting efficiency was 92%, providing 55 TEMPO radicals per polymer chain. The rest 45 carboxylic acid groups on P1 were then coupled with *N*,*N*′-dimethylaminoethyl amine (DMEA) to afford polymer P2. Compared to P1, new peaks at 2.3−2.6 and 3.3 ppm were ascribed to the tertiary amine groups, indicating a 93% conversion or 42 tertiary amine groups per polymer chain (Figure 1b). P2 was then converted into positively charged polyelectrolyte P3 through quaternization of the tertiary amines with iodomethane (Scheme 1). To avoid the interference of I$^-$ ions in electrochemical reactions, P3 was treated with an anion-exchange resin to replace iodide with chloride ions. The broad peak at 2.3−2.6 ppm in P2 shifted to 3.2−3.5 ppm in P3, suggesting the quantitative conversion of tertiary amines to ammonium ions, providing 42 positively charged units in P3 (Figure 1c). In parallel, the tertiary amines on P2 were also converted to trimethylamine *N*-oxide groups,[17] resulting in the zwitterionic radical polyelectrolytes P4. Overoxidation was avoided by using Na_2WO_4 and H_2O_2 instead of *m*-chloroperoxybenzoic acid (mCPBA), as the latter could convert a TEMPO radical to an oxoammonium cation.[28,29] Consistent with this selective oxidation, no noticeable oxoammonium peak was observed between 1550 and 1650 cm^{-1} in ATR-IR spectra, suggesting that the radicals in P4 remained intact (Figure S3).[29] The enhancement of the peak at 3.3 ppm in P4 was consistent with the formation of the target *N*-oxide. The oxidation efficiency was nearly quantitative, providing 42 *N*-oxide units per polymer chain in P4 (Figure 1d).

https://doi.org/10.1021/acs.macromol.2c00519
Macromolecules 2022, 55, 5733−5743

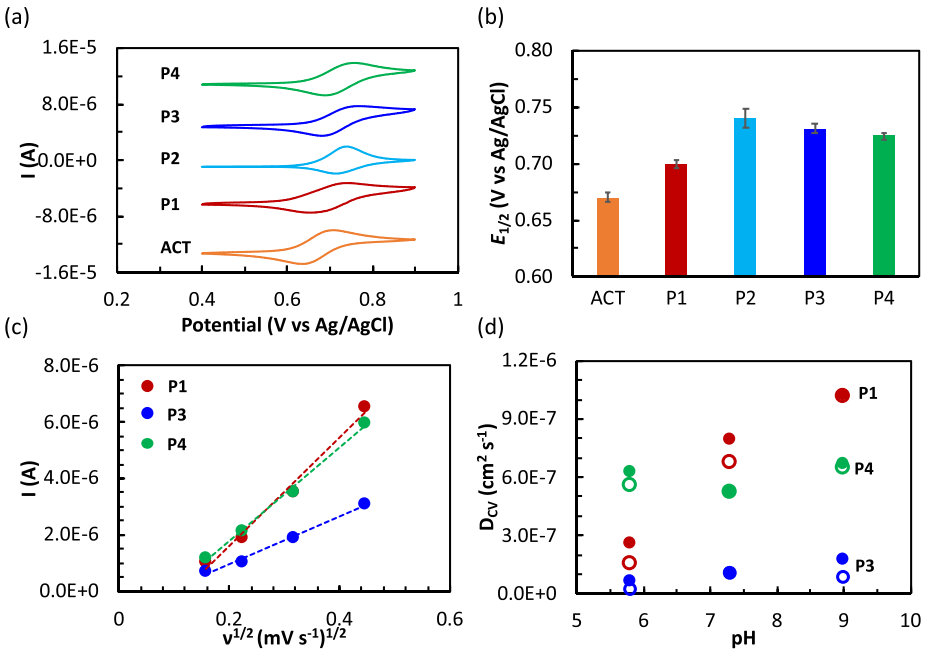

Figure 3. Cyclic voltammetry characterization radical polyelectrolytes P1−P4 and ACT in buffers. (a) Typical comparison of cyclic voltammograms of P1−P4 with ACT at pH 7.3. (b) Average redox potentials based on Table S1 (c) Randles−Sevcik plot of P1, P3, and P4 at pH 7.3. (d) Diffusion coefficient (D_{CV}) of P1, P3, and P4 derived from CV measurement at different pH (solid, based anodic current; open, based on cathodic current). The TEMPO radical concentration for all polymers was 1.0 mM in 0.1 M NaCl at pH 7.3.

Colloidal Properties of Radical Polyelectrolytes. Since the carboxylic acid and tertiary amine groups in P1 and P2 are weak acids and weak bases, respectively, we next conducted colloidal characterizations of P1 to P4 in buffer solutions with 0.1 M of NaCl. The acidic phosphate buffer at pH 5.8 was close to the pK_a of PAA but not very acidic to avoid the possible disproportionation of nitroxide radicals.[30] The basic carbonate buffer at pH 9.0 is well above the pK_a of the tertiary amine groups (approximately 7.5).[31] Previous studies showed that the diffusion coefficient of sodium polyacrylate (PAANa) decreased with increasing pH, as the electrostatic repulsion of charged chain segments is strong enough to stretch the polymer chains.[32] Here, we did not observe such a trend for P1 because, at the lower pH, P1 (with 55% of hydrophobic TEMPO groups) started to aggregate (Figure S4). When the pH increased above the pK_a of PAA (i.e., 5−6),[33] P1 was well solubilized in water and the polymer chains may not stretch out as PAA due to the randomly distributed TEMPO units weakening the intramolecular repulsion. As such, the diffusion coefficient of P1 measured by DLS (D_{DLS}) at different pH were very similar (Figure 2a). In fact, D_{DLS} for all polymers were relatively close except for P2, which showed the smallest D_{DLS} at pH 9.0 due to large aggregations formed above its pK_a (Figure S4). This ionic effect on the diffusion coefficient (D_{DLS}) of P1−P4 is consistent with their zeta potentials illustrated in Figure 2b. P1 showed a zeta potential of −15 mV at pH 5.8 and became slightly more negative to −16 mV in pH 7.3 and 9.0 buffer solution, due to nearly quantitative dissociation of PAA units. P3, with permanent positive charges, had a zeta potential of about +11 mV, and P4, with *N*-oxide groups, showed slightly negative potentials of −1.4 to −6.4 mV at pH values of 5.8 and 9.0, respectively. While the results agreed with previous reports of zwitterionic polymers,[34] we believe that the slightly decreased zeta potentials of P4 could result from a small proportion of unreacted PAA units, which would be ionized at elevated pH. This explanation also agreed with changes in zeta potentials of P2 from +12.4 to +8.0 to −5.0 mV at pH values of 5.8, 7.3, and 9.0, due to the deprotonation of both tertiary amines and carboxylic acids at the highest pH.[35] While the zeta potentials are derived from mobility, the latter more directly reflects the electrophoretic behavior. P1 and P3 displayed mobility of approximately 1.0 × 10^{-8} m^2 V^{-1} s^{-1}, showing a trend similar to their zeta potentials. Notably, the mobility for P4 was also 0.5−1.0 × 10^{-8} m^2 V^{-1} s^{-1} and close to P3, even though their absolute zeta potentials were much smaller. This result suggests that fewer electrostatic interactions between polyelectrolytes and counterions in zwitterionic P4 exert a small dragging effect on the polymer colloids, thus large mobility.[16] The absolute zeta potentials of these polyelectrolytes were less than 30 mV, indicating a propensity for weak colloidal stability. Therefore, subsequent electrochemical experiments were carried out in a dilute solution at a TEMPO concentration of 1 mM, equivalent to a polymer concentration of approximately 0.3 g L^{-1}.

Electrochemistry Behavior of Radical Polyelectrolytes in Aqueous Media. Postpolymerization modification of PAA with 4-amino-TEMPO created amide linkages between TEMPO radicals and the polymer backbone. Electrochemical studies of these polymers were compared with their small molecule analogue, 4-acetyl-TEMPO (ACT). Since both ACT and polymers possess the same amide group at the 4-position on the six-membered ring of the TEMPO radical, it eliminated the substitution effect.[36] Cyclic voltammetry (CV) was used to determine their formal redox potentials ($E^0 \approx E_{1/2} = (E_{pa}+E_{pc})/2)$) (Table S1). Figure 3a displays a typical comparison of CVs at pH 7.3 with the TEMPO concentration at 1 mM. While P1, P3, and P4 show similar cathodic and anodic peaks as ACT, P2 presents a smaller cathodic current than the anodic one due to the oxidation of tertiary amine

https://doi.org/10.1021/acs.macromol.2c00519
Macromolecules 2022, 55, 5733−5743

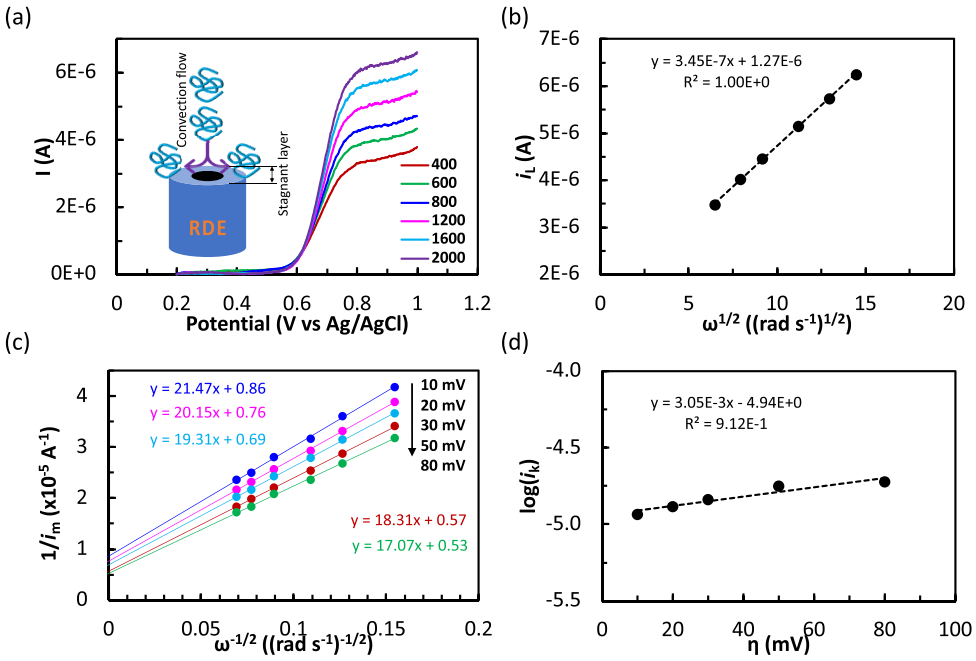

Figure 4. RDE measurements of P1 in a pH 7.3 buffer with 0.1 M NaCl and analysis. (a) Linear scan voltammograms of P1 (TEMPO radical concentration at 1.0 mM) at 10 mV s^{-1} at various rotation speeds from 400 to 2000 rpm. (b) The Levich plot of limiting currents (adopted at 0.9 V vs Ag/AgCl) vs the square roots of rotation rates. (c) The Koutecký-Levich plot for different overpotentials η to obtain the kinetic current i_k (when $\omega^{-1/2}$ approaches zero). (d) The Tafel plot of kinetic currents i_k vs overpotentials η to obtain the heterogeneous electron transfer rate constant k^0.

groups catalyzed by the oxoammonium group, the oxidized form of TEMPO.[37,38] Such an electrochemical-chemical reaction is further evidenced by the gradual disappearance of cathodic peaks when decreasing the scan rate from 50 to 10 mV s^{-1} (Figure S5). When comparing the redox potential of all polymers, there was only a mild difference for a specific radical polyelectrolyte at different pH (Table S1). However, the polymer backbone and ions moderately increase the redox potential of polymers compared with ACT (0.67 V) (Figure 3B). Previous work by Frontana and Cardoso has demonstrated the presence of different microstructures (i.e., tactical arrangement of TEMPO groups) in radical polymers altered their redox potential.[39] They also found that with the oxidation of TEMPO radicals to oxoammonium cations, the polymer chain with more positively charged groups showed an increased redox potential owing to the electron-withdrawing effect from oxoammonium groups. Therefore, we propose that the increase of redox potentials could result from a combinational effect of the polyacrylamide backbone and ionic effect, both of which dictate the redox process. The former contributes to the higher redox potential of polymers than ACT. While the latter leads to the discrepancy between P1−P4 through long-distance electronic inductive effect from ionic units, the negatively charged P1 experienced an electron-donating effect showing slightly lower $E_{1/2}$ of 0.70 V than that of P2 and P3 (i.e., 0.73 V) an electron-withdrawing effect. Additionally, the electrostatic repulsion or attraction between ionic groups and oxoammonium cations could alter polymer conformations and affect the orientation of the TEMPO radicals for electron transfer.[40] Because of the side reaction and low solubility of P2 in pH 9.0 buffer solution, we could not reliably obtain its electrochemical parameters (Figure S6); therefore, the following electrochemical studies focused on P1, P3, and P4.

The diffusion coefficients (D_{CV}) measured by CV were derived from the Randles−Sevcik equation (eq 1) through the plot of peak currents, i_p, (A) versus the square roots of scan rates, v, (V s^{-1}) (Figure 3c) and illustrated in Figure 3d.

$$i_p = 2.69 \times 10^5 n^{3/2} A D_{CV}^{1/2} C v^{1/2} \quad (1)$$

where n = 1 is the electron transfer number, A is the electrode area (0.07 cm^2), and 3.0−3.6 mg radical polyelectrolytes were dissolved in 10 mL of buffer to make the TEMPO radical concentration of C of 1.0×10^{-6} mol cm^{-3}. For a given radical polyelectrolyte at a defined condition (i.e., pH and ion strength), D_{CV} for the anodic and cathodic processes were similar in value, suggesting a quasi-reversible redox reaction (Table S1). In fact, the measured diffusion of radical polyelectrolytes under an applied potential bias (D_{CV}) is a combined effect of the Brownian diffusion (D_{DLS}) and migration through a field-induced directed motion (FIDM). For charged small molecule analytes, migration could be suppressed by adding excess inert electrolytes. As to ionic RAPs, such as radical polyelectrolytes, migration under electric field, that is, FIDM, could remain significant.[25] It is expected that D_{CV} for radical polyelectrolytes consisting of different ions could be drastically disparate. When measured under the same condition, D_{CV} of P1, P3, and P4 at various pH were mostly higher than those D_{DLS}, suggesting possible migration contributions exerted by the FIDM to the total mass transport (Table S1). This is particularly the case for P1 as D_{DLS} values were 4−6 × 10^{-8} cm^2 s^{-1} and relatively constant at three pH values (Figure 2a), but D_{CV} values were one order of magnitude greater than D_{DLS}. Moreover, D_{CV} of P1 increased significantly from ∼2.0 × 10^{-7} to ∼1.0 × 10^{-6} cm^2 s^{-1} with pH increasing from 5.8 to 9.0 (Figure 3d), primarily because of increased ionization of carboxylic acids resulting in polymers that are more attractive to the electrode. While D_{CV} values for

https://doi.org/10.1021/acs.macromol.2c00519
Macromolecules 2022, 55, 5733−5743

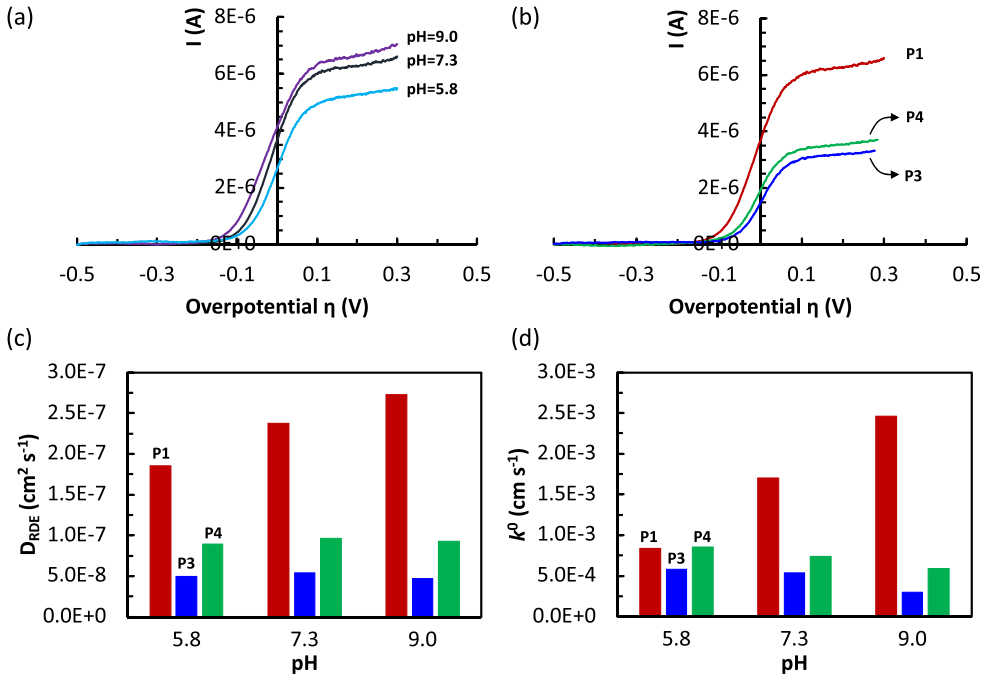

Figure 5. LSV curves normalized to their $E_{1/2}$ for (a) P1 in buffer solution at different pH and (b) P1, P3, and P4 at pH 7.3 buffer solution; all voltammograms were recorded at a rotating rate of 2000 rpm. A comparison of (c) diffusion coefficient (D_{LSV}) obtained from the Levich plots (eq 2) and (d) heterogeneous electron transfer rate constants (k^0) obtained from the Koutecký–Levich equation (eq 3), the Tafel plots, and the Butler–Volmer equation (eq 4) for P1, P2, and P3 at three different pH buffer solutions. The TEMPO radical concentration was 1.0 mM.

positively charged P3 were relatively close to those D_{DLS}, those of zwitterionic P4 were four to six times higher than D_{DLS} because of their comparable electrophoretic mobility illustrated in Figure 2c. Notably, D_{CV} for both P3 and P4 were relatively constant at three different pHs because of their less sensitivity. Such electrostatic attraction or repulsion effects found in P1 and P3 were more prominent than in zwitterionic P4, explaining that the redox potential $E_{1/2}$ and D_{CV} of P4 were somewhere between negatively charged P1 and positively charged P3 at elevated pH (i.e., 7.3 and 9.0). Although this long-range electrostatic force that influences the diffusion of radical polyelectrolytes is based on the charge types and ionic strength (not too much different here, 0.22–0.33 mol/L), CV measurements could overestimate the results due to the electrical double layer (EDL) effect, which could also complicate the determination of electron transfer kinetics.

Electron transfer kinetics of RAPs are vitally important for battery applications. Therefore, we next tried to understand how the charges on radical polyelectrolytes influence their electron transfer kinetics. Linear sweep voltammetry (LSV) at a rotating disk electrode (RDE) was carried out to (i) provide a defined thickness of the hydrodynamic boundary layer, which does not change with time, and (ii) minimize the EDL effect during the potential sweeping. The convection flow brings charged polymer chains from bulk solution into the boundary layer at the electrode surface to reach a steady state, known as the stagnant layer (Figure 4a). This hydrodynamic boundary layer δ_H has a thickness between 250 and 500 μm depending on the rotating rates. The diffusion layer thickness, δ_D, is much smaller than the stagnant layer, inside which polymer chains remain diffuse to the close proximity of the electrode for the electron transfer reaction (Figure S7). Notably, the rotating speed could change the chain conformation of radical polyelectrolytes, thereby influencing the charge transfer at the electrode surface and charge self-exchange. While increased rotating speed can induce large conformational changes, the polymer chains could be rapidly swept away from the electrode. At the low rotating rate, polymer chains stay longer at the electrode surface, but the conformational changes would be also minor. We, therefore, suppose that the overall impact of RDE on the electron transfer at the electrode surface could be relatively constant. LSV combined with RDE provides a more reliable means to obtain the diffusion coefficient, D_{RDE}, and heterogeneous electron transfer rate constant, k^0, of RAPs, enabling us to elucidate a more accurate impact of charges on the electrochemical behaviors. LSV with an RDE of P1, P3, and P4 were tested in three buffer solutions at a TEMPO radical concentration of 1 mM. Figure 4a showed typical LSV curves at different rotating speeds, from which limiting currents (i_L) were taken at a potential of 0.9 V vs Ag/AgCl. From the Levich plot, we can derive the diffusion coefficients (D_{RDE}) through the Levich equation (eq 2)

$$i_L = 0.62nFAD_{RDE}^{2/3}\upsilon^{-1/6}C\omega^{1/2} \quad (2)$$

where $n = 1$ is the number of electron transfer, F is the Faraday constant (96485 C s^{-1}), A is the electrode area (0.07 cm^2), υ is kinematic viscosity (1.01×10^{-2} cm^2 s^{-1} for the 0.1 M buffer solution), C is the TEMPO radical concentration (10^{-6} mol cm^{-3}), and ω is the angular rotation rate of the electrode (rad s^{-1}). From the CV of radical polymers in buffers, we determined their $E_{1/2}$ at 10 mV s^{-1}, and then used it to obtain the measured currents (i_m) at different overpotentials (η) from LSV curves. Figure 4c illustrated a typical Koutecký–Levich plot (eq 3) with the overpotential η from 10 to 80 mV. The kinetic currents (i_k) were obtained when $\omega^{-1/2}$ approached zero (i.e., very high rotating speed to reach maximum mass transfer) through their intercepts of each linear fit.

https://doi.org/10.1021/acs.macromol.2c00519
Macromolecules 2022, 55, 5733–5743

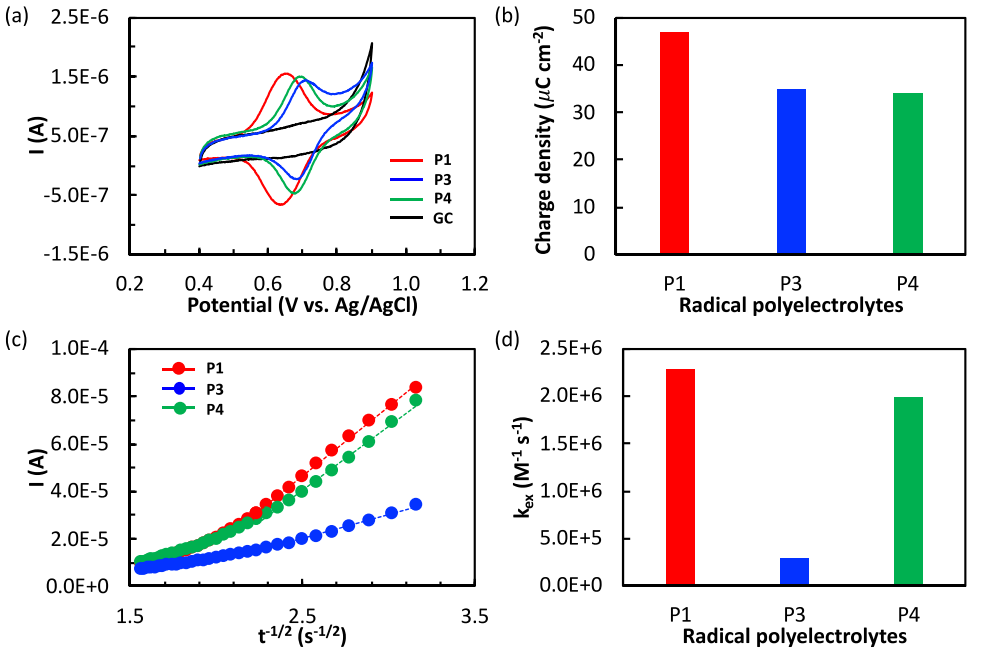

Figure 6. (a) CV curves of adsorption films of P1, P3, P4, and blank electrode in pH 9.0 at 50 mV s^{-1}. (b) Calculated surface concentration of adsorption films according to Figure S20. (c) Cottrell plots $i = nFACD_{et}^{1/2}/(\pi t)^{1/2}$ of adsorption films of P1, P3 and P4 with a potential step from 0 to 0.8 V vs Ag/AgCl, and (d) the calculated k_{ex} according to the Dahms−Ruffs equation.

$$\frac{1}{i_m} = \frac{1}{i_k} + \frac{1}{i_L} \tag{3}$$

The Tafel plot was then achieved by plotting the $\log(i_k)$ against the corresponding overpotentials. The exchange current i_0 was derived by extrapolating the linear fit to get the intercept, that is, $\eta = 0$ (Figure 4d). The heterogeneous electron transfer rate constant k^0 was obtained through the Butler−Volmer equation (eq 4)

$$i_0 = nFACk^0 \tag{4}$$

All three polymers P1, P3, and P4, were tested in three pH buffer solutions (Figure S8−S16). The diffusion coefficients from LSV (D_{LSV}) and rate constant k^0 were listed in Table S1. Figure 5a showed the LSV curves of P1 recorded at a rotating speed of 2000 rpm in different pH buffer solutions and corrected according to their redox potential $E_{1/2}$. At $\eta = 0$, a significant increase of exchange current was observed when increasing pH, suggesting an inherent increase of k^0. Whereas at a large overpotential ($\eta > 0.2$ V), the increasing currents indicated an increased diffusion coefficient (D_{LSV}) when P1 was largely ionized at a higher pH. A similar trend was observed when comparing P1, P3, and P4 in the same buffer (i.e., pH = 7.3) at the same rotating speed (2000 rpm). P1 displayed a much higher exchange current than P4, followed by P3, because of the nearly full ionization of carboxylates being more attractive to the electrode surface. When the three polymers were tested in three different buffer solutions, we obtained a full spectrum of D_{LSV} and k^0 (Figures 5c and 5d). Since RDE measurements minimize the influence of mass transfer, D_{LSV} thus reflects how different charges on these radical polyelectrolytes diffuse at the electrode surface. P3 and P4 demonstrated diffusion coefficients of $\sim 5 \times 10^{-8}$ cm^2 s^{-1} and 1×10^{-7} cm^2 s^{-1}, respectively, close to previous reports.[11,20] Notably, the pH of the buffer only exerted a small influence on the diffusion and electron transfer of permanently charged P3 and P4. Still, it altered D_{LSV} and k^0 of P1 through its pH-responsive carboxylic acid groups. At pH 9.0, P1 diffused three to five times faster (2.69×10^{-7} cm^2 s^{-1}) than P3 and P4, and the electron transfer rate constants k^0 (2.35×10^{-3} cm s^{-1}) were five to ten times higher than P3 and P4 (Figure 5c and 5d). Presumably, the negatively charged chain segments in P1 coordinate the fast reorganization of TEMPO units at the positively charged anode surface. Together with the contribution of anion self-doping,[41] a rapid electron transfer process is achieved.

Electrochemistry of Surface-Adsorbed Radical Polyelectrolyte Films. Physisorption of RAPs on the electrode surface has been observed in previous research.[9,24,25] If the adsorption occurs, the electron transfer is then mediated by the self-exchange between the adsorbed polymer layer and solubilized polymer chains. Physical adsorption of these polyelectrolytes may occur even prior to charge transfer by an adsorbate-induced electric double layer, a phenomenon of the electrode that is characteristic with the potential of zero charge (E_{pzc}).[42] To investigate the E_{pzc} effect, we carried out potential-impedance experiments to find out the E_{pzc} corresponding to the minimum differential capacitance C_{diff} for both glassy carbon and platinum electrodes in all three buffer solutions with or without P1 (Figure S17).[43] It was found that there were no noticeable changes in E_{pzc} values, even when increasing the concentration of buffer solution from 0.1 to 1.0 M. Moreover, switching the working electrode from glassy carbon to Pt did not induce a noticeable shift of peak potentials (Figure S18), suggesting a minor or undetectable E_{pzc} effect on polymer adsorption. However, the adsorption could occur before the redox reaction takes place and might be different for radical polyelectrolytes with different ions. We then carried out CV experiments in a P1 solution with different potential windows to test the adsorption behavior. It was found

https://doi.org/10.1021/acs.macromol.2c00519
Macromolecules 2022, 55, 5733−5743

that the adsorption predominately occurs during the redox reaction (i.e., 0.4 to 0.9 V vs Ag/AgCl), and only minor adsorption was observed prior to the electron transfer (i.e., −0.4 to 0.4 V vs Ag/AgCl) (Figure S19). Therefore, the adsorption experiments were carried out during the redox reaction to investigate the interactions between polymers and electrode surfaces. It is noted that the adsorbed film also acts as an active layer that mediates the electrolysis of radical polyelectrolytes in the solution through a bimolecular self-exchange reaction.

Rodriguez-Lopez[9] reported adsorption of positively charged viologen polymer on the electrode surface during the reduction process. The adsorption is believed to form a film as the surface charge density was more than 100 μC cm^{-2}, a value much higher than the monolayer (i.e., 10 μC cm^{-2}). Here, a GC working electrode was exposed to radical polyelectrolyte solutions of P1, P3, and P4 at 1 mg mL^{-1} in pH 9.0 buffer. The electrode was subjected to five cycles of CV scanning at 50 mV s^{-1}. The electrode was carefully rinsed with Milli-Q water and immersed in a blank pH 9.0 buffer. The resulting CV showed a typical redox peak of TEMPO with formal redox potentials similar to those measured in the solution (Figure 3a). Notably, the very symmetrical redox peaks and the proportional increase of peak current to the scan rates suggest a surface-adsorbed polymer layer, enabling an estimation of the surface radical concentration of polyelectrolyte films (Figure S20). It was found that P1 showed 45.8 μC cm^{-2}, 50% higher than P3 and P4 (~30 μC cm^{-2}). Interestingly, when CV measurements were run with an RDE, more prominent adsorption for P1 (57.5 μC cm^{-2}) was found (Figure S21), possibly because of the convection flow eliminating the concentration gradient impact and the opposite charge interaction now dominating the adsorption process. Next, chronoamperometry (CA) experiments were conducted for those adsorbed films that formed without using RDE (Figure S22) as their thickness were very close (Figure 6b). From the Cottrell plots of P1, P3, and P4, we could obtain the charge diffusion coefficient D_{et} for a semi-infinite diffusion process by fitting the early stage of the current decay (i.e., 0.1−0.2 s) (Figure 6c).[44] Using the Dahms−Ruffs equation,[45] we then calculate the bimolecular self-exchange rate constant (k_{ex}) (Figure 6d). k_{ex} for the negatively charged P1 (2.28×10^6 M^{-1} s^{-1}) and zwitterionic P4 (1.98×10^6 M^{-1} s^{-1}) were found to be nearly one order of magnitude greater than the positively charge P2 (2.83×10^5 M^{-1} s^{-1}). While all k_{ex} values lie in the range of 10^4−10^6 M^{-1} s^{-1} and are consistent with the previous report,[44] our system could reveal the charge impact of polyelectrolytes on the self-exchange reaction kinetics. Since the chain segments could be separate because of the swelling capability of radical polyelectrolytes, the negatively charged P1 and zwitterionic P4 could form polyelectrolyte complexes with oxoammonium cations (i.e., the oxidized state of TEMPO radicals) and bring the chain segments closer. The hopping distance between two redox centers (δ) for P1 and P4 could be much smaller than P3, resulting in smaller outer reorganization energy approximated according to the Marcus theory.[44,46] In addition, the enhancement of kinetics for P1 could also be attributed to the anion self-doping, which has been evidenced recently.[41,47] These results provided evidence of an enhanced electrochemistry process for a negatively charged radical polyelectrolyte (i.e., anodic electrochemistry process), inspiring future work on verifying their electrochemical performance in ARFBs.

CONCLUSION

In conclusion, we have synthesized a library of new radical polyelectrolytes with a controlled number and distributions of TEMPO radicals through a sequential postpolymerization modification method. These radical polyelectrolytes—with either negative, positive, or zwitterionic groups—displayed very different hydrodynamic and electrochemical properties. Colloidal characterization and electrochemical measurements with the aid of a rotating disk electrode revealed that radical polyelectrolytes consisting of carboxylic acids (P1) demonstrated a strong pH dependence for diffusion and electron transfer kinetics. The formal redox potential of P1 (0.70 V vs Ag/AgCl) was slightly higher than the small molecule analogue ACT (0.67 V), but lower than P3 (0.73 V) and P4 (0.72 V). At higher pH, P1 showed five to ten folds larger D (2.69×10^{-7} cm^2 s^{-1}) and k^0 (2.35×10^{-3} cm s^{-1}) values than the cationic polymer P3. Zwitterionic polymer P4, however, had D of 1×10^{-7} cm^2 s^{-1} and k^0 of approximately 7×10^{-3} cm s^{-1}, somewhere between P1 and P3. It is believed that the negatively charged P1 experienced stronger electrostatic attraction to the anode surface during the oxidation reaction, reducing the outer reorganization energy for heterogeneous electron transfer reaction. Such electrostatic attraction also reduced the hopping distance between TEMPO species and enable a self-doping between oxoammonium cations and carboxylate anions, resulting in the bimolecular self-exchange reaction rate of P1 and P4 ($k_{ex} \sim 2 \times 10^6$ M^{-1} s^{-1}) being approximately one order of magnitude larger than P3. The results suggested that the charges in radical polyelectrolytes could be strongly influential in electron transfer kinetics, presumably through changing polymer conformations. This work manifests the importance of considering charges in designing RAPs for their electrochemical applications in aqueous media.

ASSOCIATED CONTENT

Supporting Information

The Supporting Information is available free of charge at https://pubs.acs.org/doi/10.1021/acs.macromol.2c00519.

Synthesis of small molecule and polymer precursors, experimental data for NMR, SEC, FT-IR, and electrochemical characterizations (PDF)

AUTHOR INFORMATION

Corresponding Author

Zhongfan Jia − *Institute for Nanoscale Science and Technology, College of Science and Engineering, Flinders University, Bedford Park, South Australia 5042, Australia;* orcid.org/0000-0001-9690-7288; Email: zhongfan.jia@flinders.edu.au

Authors

Yanlin Shi − *Australian Institute for Bioengineering and Nanotechnology, University of Queensland, Brisbane, Queensland 4072, Australia;* orcid.org/0000-0003-3596-6748

Chanaka J. Mudugamuwa − *Institute for Nanoscale Science and Technology, College of Science and Engineering, Flinders University, Bedford Park, South Australia 5042, Australia*

Thidas N. Abeysinghe − *Institute for Nanoscale Science and Technology, College of Science and Engineering, Flinders University, Bedford Park, South Australia 5042, Australia*

https://doi.org/10.1021/acs.macromol.2c00519
Macromolecules 2022, 55, 5733−5743

Yasser S. M. Alotaibi − *Institute for Nanoscale Science and Technology, College of Science and Engineering, Flinders University, Bedford Park, South Australia 5042, Australia*

Michael J. Monteiro − *Australian Institute for Bioengineering and Nanotechnology, University of Queensland, Brisbane, Queensland 4072, Australia;* orcid.org/0000-0001-5624-7115

Justin M. Chalker − *Institute for Nanoscale Science and Technology, College of Science and Engineering, Flinders University, Bedford Park, South Australia 5042, Australia;* orcid.org/0000-0002-7504-5508

Jodie L. Lutkenhaus − *Artie McFerrin Department of Chemical Engineering, Texas A&M University, College Station, Texas 77843, United States;* orcid.org/0000-0002-2613-6016

Complete contact information is available at: https://pubs.acs.org/10.1021/acs.macromol.2c00519

Author Contributions

‡Y.S. and C.J.M. contributed equally. The manuscript was written through contributions of all authors. All authors have given approval to the final version of the manuscript.

Notes

The authors declare no competing financial interest.

■ ACKNOWLEDGMENTS

Z.J. acknowledges the financial support from Flinders University through the Start-up Fund. J.L. acknowledges the support from NSF Grant No. 2119672.

■ REFERENCES

(1) Leung, P.; Shah, A. A.; Sanz, L.; Flox, C.; Morante, J. R.; Xu, Q.; Mohamed, M. R.; Ponce de León, C.; Walsh, F. C. Recent developments in organic redox flow batteries: A critical review. *J. Power Sources* **2017**, *360*, 243−283.

(2) Li, B.; Liu, J. Progress and directions in low-cost redox-flow batteries for large-scale energy storage. *Natl. Sci. Rev.* **2017**, *4* (1), 91−105.

(3) Wei, X.; Pan, W.; Duan, W.; Hollas, A.; Yang, Z.; Li, B.; Nie, Z.; Liu, J.; Reed, D.; Wang, W.; Sprenkle, V. Materials and Systems for Organic Redox Flow Batteries: Status and Challenges. *ACS Energy Lett.* **2017**, *2* (9), 2187−2204.

(4) Ye, R.; Henkensmeier, D.; Yoon, S. J.; Huang, Z.; Kim, D. K.; Chang, Z.; Kim, S.; Chen, R. Redox Flow Batteries for Energy Storage: A Technology Review. *J. Electrochem. Energy Convers. Storage* **2018**, *15* (1), 010801.

(5) Li, Z.; Lu, Y. C. Material Design of Aqueous Redox Flow Batteries: Fundamental Challenges and Mitigation Strategies. *Adv. Mater.* **2020**, *32* (47), No. e2002132.

(6) Lin, K.; Gómez-Bombarelli, R.; Beh, E. S.; Tong, L.; Chen, Q.; Valle, A.; Aspuru-Guzik, A.; Aziz, M. J.; Gordon, R. G. A redox-flow battery with an alloxazine-based organic electrolyte. *Nat. Energy* **2016**, *1* (9), 16102.

(7) Chen, H.; Cong, G.; Lu, Y.-C. Recent progress in organic redox flow batteries: Active materials, electrolytes and membranes. *J. Energy Chem.* **2018**, *27* (5), 1304−1325.

(8) Montoto, E. C.; Nagarjuna, G.; Moore, J. S.; Rodríguez-López, J. Redox Active Polymers for Non-Aqueous Redox Flow Batteries: Validation of the Size-Exclusion Approach. *J. Electrochem. Soc.* **2017**, *164* (7), A1688−A1694.

(9) Nagarjuna, G.; Hui, J.; Cheng, K. J.; Lichtenstein, T.; Shen, M.; Moore, J. S.; Rodríguez-López, J. Impact of Redox-Active Polymer Molecular Weight on the Electrochemical Properties and Transport Across Porous Separators in Nonaqueous Solvents. *J. Am. Chem. Soc.* **2014**, *136* (46), 16309−16316.

(10) Burgess, M.; Moore, J. S.; Rodriguez-Lopez, J. Redox Active Polymers as Soluble Nanomaterials for Energy Storage. *Acc. Chem. Res.* **2016**, *49* (11), 2649−2657.

(11) Janoschka, T.; Martin, N.; Martin, U.; Friebe, C.; Morgenstern, S.; Hiller, H.; Hager, M. D.; Schubert, U. S. An aqueous, polymer-based redox-flow battery using non-corrosive, safe, and low-cost materials. *Nature* **2015**, *527* (7576), 78−81.

(12) Dobrynin, A. V.; Rubinstein, M. Theory of polyelectrolytes in solutions and at surfaces. *Prog. Polym. Sci.* **2005**, *30* (11), 1049−1118.

(13) Muthukumar, M. 50th Anniversary Perspective: A Perspective on Polyelectrolyte Solutions. *Macromolecules* **2017**, *50* (24), 9528−9560.

(14) Trachsel, L.; Ramakrishna, S. N.; Romio, M.; Spencer, N. D.; Benetti, E. M. Topology and Molecular Architecture of Polyelectrolytes Determine Their pH-Responsiveness When Assembled on Surfaces. *ACS Macro Lett.* **2021**, *10* (1), 90−97.

(15) Zhang, R.; Zhang, Y.; Antila, H. S.; Lutkenhaus, J. L.; Sammalkorpi, M. Role of Salt and Water in the Plasticization of PDAC/PSS Polyelectrolyte Assemblies. *J. Phys. Chem. B* **2017**, *121* (1), 322−333.

(16) Netz, R. R. Polyelectrolytes in Electric Fields. *J. Phys. Chem. B* **2003**, *107* (32), 8208−8217.

(17) Li, B.; Jain, P.; Ma, J.; Smith, J. K.; Yuan, Z.; Hung, H.-C.; He, Y.; Lin, X.; Wu, K.; Pfaendtner, J.; Jiang, S. Trimethylamine N-oxide−derived zwitterionic polymers: A new class of ultralow fouling bioinspired materials. *Sci. Adv.* **2019**, *5* (6), No. eaaw9562.

(18) Dai, J.; Zhao, H.; Lin, X.; Liu, S.; Liu, Y.; Liu, X.; Fei, T.; Zhang, T. Ultrafast Response Polyelectrolyte Humidity Sensor for Respiration Monitoring. *ACS Appl. Mater. Interfaces* **2019**, *11* (6), 6483−6490.

(19) Lee, S. W.; Kim, B. S.; Chen, S.; Shao-Horn, Y.; Hammond, P. T. Layer-by-layer assembly of all carbon nanotube ultrathin films for electrochemical applications. *J. Am. Chem. Soc.* **2009**, *131* (2), 671−9.

(20) Hagemann, T.; Strumpf, M.; Schröter, E.; Stolze, C.; Grube, M.; Nischang, I.; Hager, M. D.; et al. Schubert, U. S., (2,2,6,6-Tetramethylpiperidin-1-yl)oxyl-Containing Zwitterionic Polymer as Catholyte Species for High-Capacity Aqueous Polymer Redox Flow Batteries. *Chem. Mater.* **2019**, *31* (19), 7987−7999.

(21) Winsberg, J.; Janoschka, T.; Morgenstern, S.; Hagemann, T.; Muench, S.; Hauffman, G.; Gohy, J. F.; Hager, M. D.; Schubert, U. S. Poly(TEMPO)/Zinc Hybrid-Flow Battery: A Novel, "Green," High Voltage, and Safe Energy Storage System. *Adv. Mater.* **2016**, *28* (11), 2238−2243.

(22) Mahinthichaichan, P.; Tsai, C. C.; Payne, G. F.; Shen, J. Polyelectrolyte in Electric Field: Disparate Conformational Behavior along an Aminopolysaccharide Chain. *ACS Omega* **2020**, *5* (21), 12016−12026.

(23) Ko, Y. H.; Kim, Y. H.; Park, J.; Nam, K. T.; Park, J. H.; Yoo, P. J. Electric-Field-Assisted Layer-by-Layer Assembly of Weakly Charged Polyelectrolyte Multilayers. *Macromolecules* **2011**, *44* (8), 2866−2872.

(24) Burgess, M.; Hernández-Burgos, K.; Simpson, B. H.; Lichtenstein, T.; Avetian, S.; Nagarjuna, G.; Cheng, K. J.; Moore, J. S.; Rodríguez-López, J. Scanning Electrochemical Microscopy and Hydrodynamic Voltammetry Investigation of Charge Transfer Mechanisms on Redox Active Polymers. *J. Electrochem. Soc.* **2016**, *163* (4), H3006−H3013.

(25) Burgess, M.; Hernandez-Burgos, K.; Schuh, J. K.; Davila, J.; Montoto, E. C.; Ewoldt, R. H.; Rodriguez-Lopez, J. Modulation of the Electrochemical Reactivity of Solubilized Redox Active Polymers via Polyelectrolyte Dynamics. *J. Am. Chem. Soc.* **2018**, *140* (6), 2093−2104.

(26) Xie, Y.; Zhang, K.; Yamauchi, Y.; Oyaizu, K.; Jia, Z. Nitroxide radical polymers for emerging plastic energy storage and organic electronics: fundamentals, materials, and applications. *Mater. Horiz* **2021**, *8* (3), 803−829.

(27) Percec, V.; Guliashvili, T.; Ladislaw, J. S.; Wistrand, A.; Stjerndahl, A.; Sienkowska, M. J.; Monteiro, M. J.; Sahoo, S. Ultrafast synthesis of ultrahigh molar mass polymers by metal-catalyzed living

radical polymerization of acrylates, methacrylates, and vinyl chloride mediated by SET at 25 degrees C. *J. Am. Chem. Soc.* **2006**, *128* (43), 14156−14165.
(28) Cella, J. A.; Kelley, J. A.; Kenehan, E. F. Nitroxide-Catalyzed Oxidation of Alcohols Using Meta-Chloroperbenzoic Acid - New Method. *J. Org. Chem.* **1975**, *40* (12), 1860−1862.
(29) Easley, A. D.; Vukin, L. M.; Flouda, P.; Howard, D. L.; Pena, J. L.; Lutkenhaus, J. L. Nitroxide Radical Polymer−Solvent Interactions and Solubility Parameter Determination. *Macromolecules* **2020**, *53* (18), 7997−8008.
(30) Nutting, J. E.; Rafiee, M.; Stahl, S. S. Tetramethylpiperidine N-Oxyl (TEMPO), Phthalimide N-Oxyl (PINO), and Related N-Oxyl Species: Electrochemical Properties and Their Use in Electrocatalytic Reactions. *Chem. Rev.* **2018**, *118* (9), 4834−4885.
(31) van de Wetering, P.; Zuidam, N. J.; van Steenbergen, M. J.; van der Houwen, O. A. G. J.; Underberg, W. J. M.; Hennink, W. E. A Mechanistic Study of the Hydrolytic Stability of Poly(2-(dimethylamino)ethyl methacrylate). *Macromolecules* **1998**, *31* (23), 8063−8068.
(32) Dolce, C.; Mériguet, G. Ionization of short weak polyelectrolytes: when size matters. *Colloid Polym. Sci.* **2017**, *295* (2), 279−287.
(33) Lahav, M.; Narovlyansky, M.; Winkleman, A.; Perez-Castillejos, R.; Weiss, E. A.; Whitesides, G. M. Patterning of Poly(acrylic acid) by Ionic Exchange Reactions in Microfluidic Channels. *Adv. Mater.* **2006**, *18* (23), 3174−3178.
(34) Wang, W.; Lu, Y.; Yue, Z.; Liu, W.; Cao, Z. Ultrastable core−shell structured nanoparticles directly made from zwitterionic polymers. *Chem. Commun.* **2014**, *50* (95), 15030−15033.
(35) Han, X.; Zhang, X.; Zhu, H.; Yin, Q.; Liu, H.; Hu, Y. Effect of Composition of PDMAEMA-b-PAA Block Copolymers on Their pH- and Temperature-Responsive Behaviors. *Langmuir* **2013**, *29* (4), 1024−1034.
(36) Zhang, K.; Noble, B. B.; Mater, A. C.; Monteiro, M. J.; Coote, M. L.; Jia, Z. Effect of Heteroatom and Functionality Substitution on the Oxidation Potential of Cyclic Nitroxide Radicals: Role of Electrostatics in Electrochemistry. *Phys. Chem. Chem. Phys.* **2018**, *20* (4), 2606−2614.
(37) Sato, K.; Ono, T.; Sasano, Y.; Sato, F.; Kumano, M.; Yoshida, K.; Dairaku, T.; Iwabuchi, Y.; Kashiwagi, Y. Electrochemical Oxidation of Amines Using a Nitroxyl Radical Catalyst and the Electroanalysis of Lidocaine. *Catalysts* **2018**, *8* (12), 649.
(38) Nelsen, S. F.; Hintz, P. J. Electrochemical oxidation of tertiary amines. Effect of structure upon reversibility. *J. Am. Chem. Soc.* **1972**, *94* (20), 7114−7117.
(39) Lopez-Pena, H. A.; Hernandez-Munoz, L. S.; Frontana-Uribe, B. A.; Gonzalez, F. J.; Gonzalez, I.; Frontana, C.; Cardoso, J. Tacticity Influence on the Electrochemical Reactivity of Group Transfer Polymerization-Synthesized PTMA. *J. Phys. Chem. B* **2012**, *116* (18), 5542−5550.
(40) Kemper, T. W.; Larsen, R. E.; Gennett, T. Relationship between Molecular Structure and Electron Transfer in a Polymeric Nitroxyl-Radical Energy Storage Material. *J. Phys. Chem. C* **2014**, *118* (31), 17213−17220.
(41) Easley, A. D.; Shaligram, S. V.; Echols, I. J.; Nixon, K.; Regen, S. L.; Lutkenhaus, J. L. Layer-by-Layer Nanoarchitectonics of Electrochemically Active Thin Films Comprised of Radical-Containing Polymers. *J. Electrochem. Soc.* **2022**, *169* (2), 020510.
(42) Zebardast, H. R.; Rogak, S.; Asselin, E. Potential of zero charge of glassy carbon at elevated temperatures. *J. Electroanal. Chem.* **2014**, *724*, 36−42.
(43) Shao, L. H.; Biener, J.; Kramer, D.; Viswanath, R. N.; Baumann, T. F.; Hamza, A. V.; Weissmuller, J. Electrocapillary maximum and potential of zero charge of carbon aerogel. *Phys. Chem. Chem. Phys.* **2010**, *12* (27), 7580−7.
(44) Sato, K.; Ichinoi, R.; Mizukami, R.; Serikawa, T.; Sasaki, Y.; Lutkenhaus, J.; Nishide, H.; Oyaizu, K. Diffusion-Cooperative Model for Charge Transport by Redox-Active Nonconjugated Polymers. *J. Am. Chem. Soc.* **2018**, *140* (3), 1049−1056.
(45) Oyaizu, K.; Nishide, H. Radical Polymers for Organic Electronic Devices: A Radical Departure from Conjugated Polymers? *Adv. Mater.* **2009**, *21* (22), 2339−2344.
(46) Bard, A. J.; Faulkner, L. R. *Electrochemical Methods: Fundamentals and Applications*; New York, Wiley, 1980.
(47) Tokue, H.; Murata, T.; Agatsuma, H.; Nishide, H.; Oyaizu, K. Charge−Discharge with Rocking-Chair-Type Li+ Migration Characteristics in a Zwitterionic Radical Copolymer Composed of TEMPO and Trifluoromethanesulfonylimide with Carbonate Electrolytes for a High-Rate Li-Ion Battery. *Macromolecules* **2017**, *50* (5), 1950−1958.

https://doi.org/10.1021/acs.macromol.2c00519
Macromolecules 2022, 55, 5733−5743